MOLECULAR BASIS OF THE BOHR EFFECT IN ARTHROPOD HEMOCYANIN

Shun Hirota[1,2], Takumi Kawahara[2], Mariano Beltramini[3], Paolo Di Muro[3], Richard S. Magliozzo[4], Jack Peisach[5], Linda S. Powers[6], Naoki Tanaka[1], Satoshi Nagao[1], and Luigi Bubacco[3]

[1] Graduate School of Materials Science, Nara Institute of Science and Technology, Nara, Japan; [2] Department of Physical Chemistry and 21st Century COE Program, Kyoto Pharmaceutical University, Kyoto, Japan; [3] Department of Biology, University of Padova, Padova, Italy; [4] Department of Chemistry, Brooklyn College, Brooklyn, NY, USA; [5] Department of Physiology and Biophysics, Albert Einstein College of Medicine, Bronx, NY, USA; [6] National Center for the Design of Molecular Function, University of Arizona, Tucson, AZ USA.

Running head: Bohr effect in Hemocyanin

Address correspondence to: Luigi Bubacco Department of Biology, University of Padova, Via Ugo Bassi 58B, Padova 35121, Italy, +390498276346, fax +390498276299, luigi.bubacco@unipd.it; Shun Hirota, Graduate School of Materials Science, Nara Institute of Science and Technology, 8916-5 Takayama, Ikoma, Nara 630-0192, Japan; +81-743-72-6110, fax +81-743-72-6119, hirota@ms.naist.jp

Flash photolysis and K-edge X-ray absorption spectroscopy (XAS) were used to investigate the functional and structural effects of pH on the oxygen affinity of three homologous arthropod hemocyanins (Hcs). Flash photolysis measurements showed that the well-characterized pH dependence of oxygen affinity (Bohr effect) is attributable to changes in the oxygen binding rate constant, k_{on}, rather than changes in k_{off}. In parallel, coordination geometry of copper in Hc was evaluated as a function of pH by XAS. It was found that the geometry of copper in the oxygenated protein is unchanged at all pH values investigated, while significant changes were observed for the deoxygenated protein as a function of pH. The interpretation of these changes was based on previously described correlations between spectral lineshape and coordination geometry obtained for model compounds of known structure (Blackburn NJ, Strange RW, Reedijk J, Volbeda A, Farooq A, Karlin KD, Zubieta J. (1989) *Inorg. Chem.*, 28: 1349-1357). A pH-dependent change in the geometry of cuprous copper in the active site of deoxyHc, from pseudotetrahedral towards trigonal was assigned from the observed intensity dependence of the $1s \rightarrow 4p_z$ transition in x-ray absorption near edge structure (XANES) spectra. The structural alteration correlated well with increase in oxygen affinity at alkaline pH determined in flash photolysis experiments. These results suggest that the oxygen binding rate in deoxyHc depends on the coordination geometry of Cu(I) and suggest a structural origin for the Bohr effect in arthropod Hcs.

Hemocyanins (Hcs) are oxygen carrier and storage proteins found in molluscs and arthropods. Significant differences are observed between mollusc and arthropods Hcs in size of the functional units and in their tertiary and quaternary structures. Specifically, arthropod Hcs are structurally homogenous oligomeric proteins with a minimal functional subunit of 75 kDa. Under physiological conditions in the presence of calcium, the subunits are typically arranged in hexamers and dodecamers. Removal of Ca^{2+} with EDTA at neutral pH causes dissociation of the dodecamer into hexamers, which can be dissociated into monomers at alkaline pH (1). The different aggregation states are related to modified oxygen binding properties (2). As generally observed for respiratory proteins, a fundamental physiological property of Hc is its competence to bind oxygen with different affinity in response to allosteric effectors including hydrogen ions.

Detailed structural information

concerning the active site of Hcs is derived mainly from a limited set of x-ray crystallographic investigations. The active site structures of the deoxy form have been described for two arthropod Hcs, *Panulirus interruptus* (3) and *Limulus polyphemus* (subunit II) (4). However, comparison of the results are limited by the different solution conditions from which the proteins were crystallized. In both examples, each Cu(I) of the binuclear active site is coordinated by the ε-nitrogen of three histidine imidazole residues. In the *P. interruptus* structure obtained from protein crystallized at pH 4.8, two of the three histidine imidazole ligands and one copper atom lie nearly in a plane, with Cu-N bond lengths of 1.9 Å. In addition, each metal atom binds to a third histidyl imidazole nitrogen at a distance of 2.7 Å, perpendicular to the plane defined by the two equatorial histidine nitrogens and a copper atom. In contrast to this, the structure of *L. polyphemus* subunit II deoxyHc, obtained from crystals grown in 0.5 M chloride at pH 6.5-7.0, shows that each copper has approximately trigonal planar coordination geometry, with three histidyl imidazole nitrogens at a distance of 1.9-2.2 Å from the copper. These ligands define a plane from which the copper is displaced by 0.3 Å. An important additional difference between these two structures is the metal-metal distance, which is 3.6 Å in *P. interruptus* Hc (low pH and low ionic strength) and 4.6 Å for *L. polyphemus* Hc (physiological pH and higher ionic strength) Fig. 1.

The only example of an oxy structure for an arthropod Hc is that of subunit II of the *L. polyphemus* protein crystallized at pH 6.2 (5). In this example, the oxygen molecule is bound as a peroxide and forms a μ:η^2-η^2 bridge between the two Cu(II) atoms. Each copper atom is penta-coordinated in a square pyramidal geometry, where the equatorial plane is now defined by two histidyl imidazole nitrogens and the bound oxygen, while a third histidyl nitrogen is axially coordinated to copper. All three Cu-N bond lengths are 1.9 Å and the metal-metal separation is 3.0-3.5 Å (6), a distance supported by EXAFS analysis for the closely related *P. interruptus* oxyHc (7, 8).

Oxygen binding to arthropods Hcs is very sensitive to pH and the relevance of this Bohr effect resides in the capability of these proteins to respond to a pH variation in the medium with a variation in affinity for molecular oxygen to meet physiological needs. Although Hc has been studied extensively, detailed information concerning oxygen binding kinetics and the origins of both cooperativity and the Bohr effect is still limited (4-6). A useful approach for the study of oxygen binding kinetics is flash photolysis. OxyHc is blue and its optical spectrum is characterized by a CT band at about 345 nm and a d-d band at about 600 nm (9-12). DeoxyHc is colorless. Taking advantage of these optical differences, a photolysis approach was previously used to study the binding of oxygen to *Streptomyces antibioticus* tyrosinase, a mononomeric enzyme that like Hc contains a binuclear copper center with similar optical properties (13).

In the present study, flash photolysis was used to investigate oxygen binding to Hc allowing us to probe allosteric effects. A complementary approach to the kinetic studies is x-ray absorption spectroscopy (XAS), which allows for the investigation of the immediate coordination geometry of Cu(I) in deoxyHc. For Cu(I), a species with limited potential for other spectroscopic studies as it lacks color and paramagnetism, coordination geometry can be deduced from copper k-edge absorbance measurements. Previous studies on Cu(I) model complexes of known structure provide the background information used to define a correlation between k-edge features and coordination geometry (14, 15).

Three paradigmatic arthropod Hcs that are structurally and functionally characterized were used here (2). Flash photolysis was used to obtain the kinetic parameters of oxygen binding, while XAS was used to define structural features of copper centers in the active site as a function of pH. The results suggest that the O_2 binding rate depends on the coordination geometry of Cu(I) in deoxyHc providing evidence for a structural origin of the Bohr effect.

Experimental Procedures

Sample preparation

P. interruptus and *C. aestuarii* Hcs were

purified and stored as previously described (1, 16).

L. polyphemus hemolymph was collected at the Marine Biological Laboratories, Woods Hole, MA. The clotted hemolymph was filtered through gauze and centrifuged to eliminate debris. The clear dark blue supernatant was dialysed overnight at 4 °C against 20 mM $CaCl_2$, pH 7.0. During dialysis, a small amount of precipitate was formed and was separated by low speed centrifugation. The individual subunits were purified according to a published method (17). Subunit II was used in this study because of its well-characterized allosteric properties (18). The purity of the protein was verified by the electrophoretic mobility while its aggregation state in the presence of Ca^{2+} was determined by analytical ultracentrifugation using Schlieren optics (18). Control oxygen binding experiments were carried out using a thin layer optical cell as previously described (19).

Flash photolysis measurements

Purified Hc of *C. aestuarii* in 50 mM Tris-HCl buffer, pH 8.3, was degassed on a vacuum line and then flushed with nitrogen gas. Hydroxylamine was added to the sample solution anaerobically (final concentration, 1 mM) in order to reduce any oxidized protein. The solution was then dialyzed under aerobic conditions against 50 mM Tris-HCl, MES or acetate buffer at the desired pH. After dialysis, the protein concentration was adjusted to 20 μM and a sample was placed under an atmosphere of oxygen plus nitrogen such that the partial pressure of oxygen could be varied from 5 to 100% with a mixed gas generator (MX-3S, Crown, Tokyo, Japan). The sample solution was filtered under the appropriate oxygen concentration and was transferred into the sealed quartz cell, which was filled with the same gas mixture.

Photolysis of oxyHc samples was accomplished using the third harmonic of an Nd:YAG laser (Surelight I-10, Continuum, Santa Clara, U.S.A; pulse energy, 30 mJ; pulse width, 5 ns) for excitation. Time-resolved absorbance changes were measured at 20°C with illumination from a Xe lamp orthogonal to the laser pulse and were recorded on a digital oscilloscope (TDS 3012B, Tektronix, Tokyo, Japan), which received voltage signals from the photomultiplier attached to a monochromator (RSP-601-03, Unisoku, Osaka, Japan). The traces were obtained as the average of 256 or 512 pulses, and least-squares exponential fits were performed for the time-resolved absorption data using Igor Pro ver. 4.0 (WaveMetrics).

X-ray edge measurements

Highly concentrated Hc (2 mM copper concentration) used in spectroscopic experiments was prepared using a Centricon filter (Amicon) and then transferred to Lucite® sample holders designed for the x-ray measurements (20). DeoxyHc was obtained by passing a pre-humidified argon stream through an air tight, homemade chamber designed to host the loaded sample holders. Through the transparent faces (top and bottom) of the chamber, it was possible to monitor the course of deoxygenation based on the disappearance of the blue colour of oxyHc. It was estimated that no more than 2-3% oxyHc remained in the apparently colourless sample by visual inspection. After deoxygenation, the sealed chamber was cooled in liquid nitrogen and the frozen sample was removed and stored at 77 K until used. All samples were placed in a 25 x 2.5 x 2 mm Lucite® sample holder covered with Kapton® tape.

X-ray fluorescence data were collected on beam lines X-9A and X-10C at the National Synchrotron Light Source (NSLS), Brookhaven National Laboratory, using double flat Si(111) (X-9A) and Si(220) (X-10C) crystal monochromators with fixed exit geometry. Beam harmonics were rejected using a nickel (X-9A) or rhodium (X-10C) coated mirror positioned downstream of the monochromator. Sample temperature was maintained at approximately 120 K by flowing cooled nitrogen gas through a Lucite® cryostat as described previously (1). X-ray edge data having 3 eV resolution (X-9A) and 2 eV resolution (X-10C) were recorded by counting at single energy values for 3 sec and incrementing the energy in 0.5 eV steps

from 30 eV below the copper edge to 120 eV above the edge. Copper foil was used as an energy standard to account for any shifts in the monochromator calibration for any individual scan. Kapton® tape was mounted at a 45° angle to the incident x-ray beam to scatter x-ray photons through the copper foil. The photons were then counted with a photomultiplier tube positioned perpendicular to the x-ray beam as previously described (1). X-ray flux was 1.0 x 10^{10} (X-9A) and 1.3 x 10^{10} photons sec^{-1} mm^{-2} at 100 mA beam current (X-10C). X-ray edge data were generally taken in the range of 100-225 mA. K-copper fluorescence was detected with a 13-element solid-state energy-resolving germanium detector, and incident photon scattering was rejected by a nickel filter. Reference signals (incident beam intensity, I_o) were collected using a standard ion chamber. In order to monitor the condition of samples after X-ray exposure, optical spectra in the UV and visible regions were collected after sample dilution in buffer. Sample integrity was verified by the ratio between the absorbance at 280 nm and the charge transfer transition of oxyHc at 345 nm. No significant difference was found in this ratio collected before and after the XAS experiments.

X-ray edge spectra were normalized by fitting a function to pre- and post-edge regions of the spectrum and normalising the edge jump to 1.0 at 9060 eV. To rule out systematic errors, partial sums of the total number of scans were independently fit without any significant differences noted.

RESULTS

Flash photolysis of oxygen from oxyhemocyanin

The absorbance change after flash photolysis of *Carcinus aestuarii* oxyHc was monitored at 337 nm, the absorption maximum of the oxyHc spectrum (Fig. 2). In order to prove that the observed optical change corresponded to oxygen photolysis and re-binding, the wavelength dependence of the initial absorbance change at several wavelengths within the absorption envelope of oxyHc was measured and this action spectrum is depicted in the inset of Fig. 2. In the same figure, the difference absorption spectrum between oxyHc and deoxyHc is shown (Fig. 2, inset dotted line), which was well correlated with the wavelength dependence of the initial absorption change after photolysis. The experimental conditions were designed such that 100% of the Hc was in the oxygenated form before photolysis at all oxygen concentrations tested (1). The fraction of deoxyHc present at the beginning of detectable oxygen re-binding was about 5% as calculated on the basis of the absorbance change. The time scale of absorbance recovery was in the range of microseconds to submilliseconds. The initial absorbance decrease corresponded to dissociation of oxygen from oxyHc, whereas the complete intensity recovery indicated re-binding of oxygen with no detectable photo damage.

The observed absorbance changes at 337 nm were fit successfully with single exponentials for all oxygen concentrations at pH 8.3. Although at this pH in the presence of Ca^{2+}, *C. aestuarii* Hc is known to be a mixture of 90% dimer of hexamers and 10% hexamers (1), there was no observable heterogeneity in the kinetic data. There was likewise no evidence for bi-phasic character that might be expected if the Hc were switching between R and T-state upon photolysis.

The observed oxygen re-binding rate constant (k_{obs}) increased upon increasing the pH from 6.5 to 8.7 (Fig. 3A). The k_{obs} values at pH 8.3 and 6.5 are plotted in Fig. 3B as a function of oxygen concentration; the dependence of k_{obs} on oxygen concentration was steeper for the measurements at pH 8.3 than that at pH 6.5. As will be discussed later, the ordinate intercept of the plots gave coincident k_{off} values, demonstrating that only the k_{on} values are pH dependent. The shape of the optical spectrum of oxyHc is pH independent, such that optical spectra at different pH values are superimposable. Therefore, our flash photolysis approach does not require any correction for pH effects on the spectrum of oxyHc.

The absorbance change upon photolysis

of oxyHc at pH 7.1 under O_2 concentrations lower than 0.35 mM could not be successfully fit with a single exponential curve (Fig. S1, supplementary material, depicts the case for $[O_2]$ = 0.14 mM), although single exponential fits were adequate for Hc at pH 8.3 under all oxygen concentrations studied, and at pH 7.1 under higher oxygen concentration ($[O_2]$ > 0.49 mM). For the samples at pH 7.1 under oxygen concentrations less than 0.35 mM, double exponential curves were required to fit the data, suggesting a second process is operative under these conditions. The cooperative homohexamers of CaeSS3 subunits of Hc (1), exhibited only a single phase at pH 7.5 and $[O_2]$ = 1.39 mM, with smaller k_{obs} values than the heterohexameric native protein (*Cae*SS3 homohexamers, 61 ± 5 ms^{-1}; the heterohexameric native protein 72.2 ± 3.2 ms^{-1}).

In order to calculate thermodynamic parameters for the oxygen re-binding reaction, we studied the temperature dependence of k_{obs}. In the tyrosinase case (13), the initial intensity change in absorbance in the photolysis experiments depended on temperature such that as the temperature increased, the intensity change increased, whereas for Hc, there was no observed temperature dependence of the optical features. These observations suggest that the structure of Hc at the active site is more rigid than that of tyrosinase (13) and that the increase in the oxygen-binding rate constant in Hc as a function of temperature is not due to protein structural changes. A linear Eyring plot was obtained based on the temperature dependence of k_{on} within the range 5 to 25 °C (Fig. 4). The activation enthalpy and entropy of oxygen binding to Hc calculated from the temperature dependence were as follows; $\Delta H^{\ddagger}$ = 7.2 kcal/mol and $\Delta S^{\ddagger}$ = -26 cal/(mol·K), respectively, based on the data in Fig. 4. These values compare reasonably well with those reported for oxygen binding to binuclear copper model complexes (21).

Copper k-edge spectra of arthropod hemocyanin

Oxy and deoxyHc have readily distinguishable x-ray absorption spectra. For example, a comparison of the copper k-edge spectra of oxy and deoxy forms of *P. interruptus* Hc (Fig. 5), a very close homolog of *C. aestuarii* Hc, indicates a shift of 2-3 eV to higher energy expected from the increase in the 1s-electron binding energy for the metal ion in the oxy protein because of its cupric character (14). The difference spectrum between deoxy and oxyHc allows for an accurate determination of the peak positions in the edge spectra of the deoxy protein. The two largest absorbance difference peaks, at 8982.7 ± 0.5 and 8985.6 ± 0.5 eV, have been assigned to the $1s \rightarrow 4p_z$ and $1s \rightarrow (s+p)^*$ transitions, respectively (15). In a separate study, the intensities of these transitions were correlated with the coordination geometry of Cu(I) based on a systematic analysis of x-ray edge spectra for a collection of model complexes having different coordination geometries but the same tridentate nitrogen ligands (20,22,24). More precisely, the intensity of the 8982.7 eV feature, normalized to the edge jump, was found to be inversely proportional to the mean displacement along the z axis of Cu(I) from the plane defined by the three directly coordinated nitrogen atoms. The intensity is significantly higher for the metal ion coordinated in a trigonal planar geometry compared to that for pseudotetrahedral geometry, in which the copper atom lies out of the plane defined by the ligands (20, 24). Therefore, the 8982.7 eV feature can serve as a spectroscopic probe of coordination geometry in Cu(I) sites with all nitrogen coordination as in deoxyHc and was used here to define the structural modifications induced by changes in pH.

The k-edge spectra for *P. interruptus* deoxyHc at different pH values are collected in Fig. 6. The oxygen affinity of this Hc increases approximately 35-fold from pH 5 to 9 (Table I) (25, 26). At pH 5.25, the intensity of the 8982.7 eV feature is low (Fig. 6 a). As the pH is raised to 7, and finally to 9, the intensity increases (Figs. 6 b and c). This spectroscopic change is indicative of the alteration of Cu(I) geometry from pseudotetrahedral towards trigonal (22). The spectral changes observed are not due to oxidation of Cu(I) to Cu(II) because the lineshape of the x-ray absorption edge spectra collected at different pH values overlay in the 9000 eV region, with no indication of an energy shift expected if Cu(I) were oxidized to Cu(II). A smaller increase in the intensity of the 8982.7

eV feature with increasing pH was noted for subunit II of *L. polyphemus* Hc (Fig. 7) compared to the data described for *P. interruptus* Hc. This protein also has a Bohr effect (18) and the structural modulation induced by pH is considered here to be analogous to that described for *P. interruptus* Hc, indicating the general nature of the observations and also establishing a correlation between the magnitude of the Bohr effect and the observed intensity changes for two different Hcs. *C. aestuarii*, *P. interruptus* and *L. polyphemus* Hcs are highly homologous and show the same trend in the pH dependence of oxygen binding.

DISCUSSION

Structural features of deoxyhemocyanin

In this study, the coordination geometry of copper in deoxyHc was investigated using x-ray spectroscopy. Data for the protein are interpreted based on k-edge absorption spectra for several Cu(I) model complexes of known structure, which show a correlation between the intensity of the 8982.7 eV ($1s \rightarrow 4p_z$) transition and geometry; high intensity corresponds to trigonal planar coordination (22, 27) and low intensity occurs for pseudotetrahedral symmetry (C_{3v}), because of mixing of s orbital character into the final state wave function (22). The observed increase in intensity of the $1s \rightarrow 4p_z$ transition with increasing pH values for both *P. interruptus* and subunit II of *L. polyphemus* deoxyHcs is interpreted as a change in coordination geometry from pseudotetrahedral at low pH towards trigonal planar at high pH. This change in structure is suggested to correlate with the Bohr effect known for the proteins investigated here. Pseudotetrahedral coordination geometry at low pH for Hc in solution is in agreement with the x-ray crystal structure of *P. interruptus* deoxyHc at pH 4.8 (2). The trigonal geometry of the high pH form of Hc cannot be corroborated by a comparison with an x-ray crystal structure as none is available at alkaline pH. It may be noted that the k-edge spectrum of Cu(I) in reduced SOD (28) closely resembles that of the high pH form of deoxyHc in terms of the relative intensity of the $1s \rightarrow 4p_z$ band compared to the edge jump. The x-ray crystal structure of reduced SOD (Pdb file1dsw) shows a trigonal coordination geometry for Cu(I), with three nearly equal Cu-N bond lengths and angles of 120° between these bonds, similar to the crystal structure for Hc at high pH. It is suggested that for deoxyHc, the changes in geometry as a function of pH and the resulting changes in oxygen affinity derive from constraints on the active site in response to changes in protein conformation.

Modulation of oxygen affinity in hemocyanin

The interplay of many factors enters into the mechanism of oxygen binding and the modulation of oxygen affinity in Hcs. These include the coordination geometry of the copper, accessibility of the active site, the Cu-Cu distance and the redox potential of the copper. The latter is important since oxygenation involves electron transfer from each Cu(I) to oxygen to yield a Cu(II)-O_2-Cu(II) structure. Allosteric effectors may influence oxygen binding by producing alterations in the tertiary and quaternary structure of the multimeric proteins and their subunits that have effects on the active site. Here, we have focused on copper (I) coordination geometry as a parameter not recognized before as one having an impact on Hc function.

The flash photolysis results provide a quantitative approach to analyze the relationship between k_{on} and oxygen affinity. The observed rate constant may be described according to eq. 1 (28):

$$k_{obs} = k_{on}([\text{deoxyHc}]+[O_2]) + k_{off} \qquad (1)$$

Since close to 100% of Hc was oxygenated in all samples (Hc concentration is 1 μM and dissolved O_2 is 220 μM or greater) and less than 5% of the total protein is monitored in the re-binding experiment, the deoxyHc concentration term can be neglected in eq. 1. Least squares fitting of a plot of k_{obs} against $[O_2]$ at pH 8.3 (Fig. 3B, black curve) using eq. 1, gives k_{on} and $k_{off} = (6.35 \pm 0.05) \times 10^7\ M^{-1}s^{-1}$ and $1{,}800 \pm 500\ s^{-1}$, respectively. From these values, the oxygen dissociation constant (K_D) was calculated as 28 ± 8 μM at pH 8.3. This K_D value was relatively close to that calculated (13 ± 1 μM) from the reported binding constant for *C.*

aestuarii Hc obtained from equilibrium measurements (1). The only other available kinetic parameters are k_{on} and k_{off} of oxygen binding in *P. interruptus* Hc obtained by temperature-jump and stopped-flow measurements, respectively (29). Although the reported K_D value for *P. interruptus* Hc is smaller (2.0–9.1 μM), most likely because the measurements were carried out in the presence of 100 mM NaCl, which is known to act as a heterotropic effector increasing oxygen affinity (30). From the temperature-jump measurement, a k_{on} value was estimated to be approximately 3.2 x 10^7 $M^{-1}s^{-1}$, which is close to the value found here, but again was measured in the presence of 100 mM NaCl.

Here, the slope of the fitted curve (Fig. 3B, red curve) for oxygen rebinding rate was lower for the data at pH 6.5 than 8.3, with a calculated k_{on} = (4.91 ± 0.06) x 10^7 $M^{-1}s^{-1}$ and k_{off} = 1,800 ± 700 s^{-1}. While the k_{off} value remains the same at the two pH values within experimental error, the k_{on} value decreases at low pH. The observed pH dependence of k_{on} may be correlated with geometric flexibility of Cu(I) which can reasonably be assumed to govern the modulation of oxygen affinity. The pH independent character of k_{off} is consistent with the pH independence of both the optical spectra of oxyHc and the k-edge absorption properties of several oxyHcs (31). These observations are also consistent with the common square pyramidal structure for copper in the oxygenated Type III copper site found in tyrosinase (32), other Hcs (33) and catechol oxidase (34). Our results lead us to suggest that the Bohr effect for arthropod Hcs derives from structural modulation of the geometry of copper in deoxyHc rather than in oxyHc, according to the scheme presented in Fig. 8.

In the flash photolysis experiment, we are observing the behaviour of a deoxygenated site in a nearly fully oxygenated R-state hexamer for the case at pH 8.3 and high oxygen concentration at pH 6.5. A plausible interpretation of the observed changes in k_{on} is that the single deoxygenated site that is part of R-state hexamers, may in the time frame of the experiment, rearrange into different structures (R′) in response to the pH of the medium such that oxygen binding is favoured at higher pH. Furthermore, oxygen binding data (1, 35) for both *C. aestuarii* and *Penaeus monodon* Hcs show that K_T and K_R both increase with pH (Fig S2, supplementary material). The structural rearrangements of the deoxy site in the R multimer can then be the origin of the pH dependence of K_R, this parameter being the oxygen dissociation constant from the R state. Therefore, it seems reasonable, and it is the simpler interpretation, that the parallel pH dependencies of K_T and K_R reported earlier arise from the same phenomenon, i.e., a change in the coordination geometry of Cu(I) in deoxygenated sites. This allows us to assume that the deoxy sites in the photolysis experiments are sensitive to pH in a similar way in a hexamer that is oxygenated or deoxygenated.

Central to this idea is the fact that all oxygenated type III structures reported from x-ray crystal data are superimposable, despite the fact that the Hcs are from organisms that belong to different *phyla* and the proteins may have been crystallized at different pH values (3-4). Oxygen dissociation occurs from this unique structure, which would explain the pH independence of k_{off} values found here. It is reasonable then to suggest that a general mechanism for arthropod Hcs to modulate oxygen affinity involves a structural rearrangement in the deoxygenated protein that produces a change in k_{on}. This conclusion is substantiated by the comparison of Fig. 6 and Fig. 7 where a greater magnitude of spectral change was observed for *P. interruptus* deoxyHc compared to *L. polyphemus* Hc. The former protein has a greater difference in oxygen affinity per pH unit change than does *L. polyphemus* Hc. In further support of this concept, it should be noted that the presence of a Bohr effect for the binding of carbon monoxide to *P. interruptus* deoxyHc (36), a ligand that binds to only one copper, can be rationalized by a change in coordination geometry of a single Cu(I) with pH. Previous suggestions have focused instead on a change in copper-copper distance to explain the phenomenon (4, 6).

During oxygen coordination, ligand reorientations must occur as the copper coordination geometry is altered from distorted

trigonal planar (or pseudotetrahedral) to square pyramidal in the Cu(II)-oxy form. A calculated reaction coordinate for reversible oxygen binding was investigated for Hc (24), and it was proposed that the protein matrix holds the Cu(I) ions in close proximity and therefore enables a simultaneous 2-electron transfer. The structural effect of pH on the individual Cu(I) sites of the binuclear center proposed here may result in a modulation of both the redox potential of the individual copper ions and also the Cu-Cu distance in agreement with a proposed two-electron reduction of molecular oxygen.

The thermodynamic data reported here show that the $\Delta H^{\ddagger}$ and $\Delta S^{\ddagger}$ values for oxygenation of Hc are comparable to those reported for the μ:η^2-η^2-peroxodicopper(II) and superoxo model compounds ($\Delta H^{\ddagger}$ = 8.9 and 7.2 kcal/mol and $\Delta S^{\ddagger}$ = -15 and –13 cal/(mol·K), respectively) (21). The similarity between the parameters for superoxo binding and peroxo binding and the overall similarities between the models and the results for Hc suggest that superoxo complex formation may be the rate limiting step and the peroxo species could be produced relatively easily from the superoxo species during the μ-η^2:η^2-peroxodicopper(II) model complex formation and during Hc oxygenation as well. The latter is in agreement with a nearly simultaneous 2 electron transfer to O_2 as previously suggested (24). Also, the similarity in the parameters for Hc and the models suggests that despite the fact that the ligand must diffuse through the protein matrix to the active site, the interactions do not have an impact on the thermodynamics of oxygen binding.

It should be mentioned that the molecular basis of the Bohr effect proposed here implicates a structural change in coordination geometry for the copper only, leaving the question of identifying the role of individual amino acids to future studies. The ionization state of amino acids throughout the Hc molecule and changes in conformation of the polypeptide involved in the Bohr effect are expected to also affect the R/T equilibrium and the Hill coefficient, which combined produce the pH dependence of the oxygen binding parameters. Salt bridges between some conserved histidine and glutamate residues on the contact surface between monomers of *Eurypelma californicum* Hc (37) are proposed to be important. Possible mediators of allosteric signals have been recently described for *L. Polyphemus* Hc (38). The deoxy protein is known to exhibit different conformations which are evident in changes in the binding of small molecule allosteric effectors. Whether pH effects on the binding of these molecules and the Bohr effect are related remain to be demonstrated (39). However, unravelling the details of the mechanism that links the active sites in the oligomers leading to conformational changes, will require further study. In conclusion, the analysis presented here provides a reasonable general explanation of the structural relationship between metal geometry and the Bohr effect in arthropod Hcs.

References

1. Dainese E, Di Muro P, Beltramini M, Salvato B, Decker H (1998). *Eur. J. Biochem.* **256**: 350-358.
2. Markl J, Decker H (1992) *Adv. Comp. Environ. Physiol.* **13**: 325-376
3. Volbeda A, Hol WGJ (1989). *J. Mol. Biol.* **209**: 249-279.
4. Hazes B, Magnus C, Bonaventura C, Bonaventura J, Dauter Z et al., (1993). *Protein Science* **2**: 567-619.
5. Magnus KA, Hazes EE, Lattman A, Volbeda A, Hol WGJ (1991). *Proteins: Struct. Funct. Gen.* **9**: 240-247.

6. Magnus KA, Hazes B, Ton-That H, Bonaventura C, Bonaventura J et al. (1994) *Proteins.* **19**: 302-309.
7. Feiters MC (1990) *Comments Inorg. Chem.* **11**: 131-174.
8. Volbeda A, Feiters MC, Vincent MG, Bouwman E, Dobson B, et al. (1989) *Eur. J. Biochem*. **181**: 669-673. .
9. Jolley RL, Jr, Evans LH, Makino N, Mason HS (1974) *J. Biol. Chem.* **249**: 335-345.
10. Heirwegh K, Borginon H, Lontie R (1961) *Biochim. Biophys. Acta* **48:** 517-526.
11. van Holde KE (1967). *Biochemistry* **6**: 93-99.
12. Solomon EI, Lowery MD (1993) *Science* **259**: 1575-1581.
13. Hirota S, Kawahara T, Lonardi E, de Waal E, Funasaki N, et al. (2005) *J. Am. Chem. Soc*. **127:** 17966-17967.
14. Cramer SP, Eccles TK, Kutzler FW, Hodgson KO, Mortenson LE (1976) *J. Am. Chem. Soc*. **98**: 1287-1288.
15. Smith TA, Penner-Hahn JE, Berding MA, Doniach S, Hodgson KO (1985) *J. Am. Chem. Soc.* **107**: 5945-5955.
16. Magliozzo RS, Bubacco L, McCracken J, Jiang F, Beltramini M, et al. (1995) *Biochemistry* **34**: 1513-1523.
17. Brenowitz, M, Bonaventura C, Bonaventura J, Gianazza E (1981) *Arch. Biochem. Biophys*. **210:** 748-761.
18. Brenowitz M, Bonaventura C, Bonaventura J (1984) *Arch. Biochem. Biophys.* **230**: 238-249.
19. Kraus DW, Wittemberg JB. (1990) *J. Biol. Chem.*, **265**:16043-53
20. Brown J.M, Powers L, Kincaid B, Larrabee JA, Spiro TG (1980) *J. Am. Chem. Soc*. **102**: 4210-4216.
21. Karlin KD, Tolman WB, Kaderli S, Zuberbühler AD (1997). *J. Mol. Catal. A: Chemical* **117**: 215-222.
22. Blackburn NJ, Strange RW, Reedijk J, Volbeda A, Farooq A et al. (1989).*Inorg. Chem.*, **28**: 1349-1357.
23. Molon A, Di Muro P, Bubacco L, Vasilyev V, Salvato et al. (2000) *Eur. J. Biochem*. **267**: 7046-7057.
24. Metz, M, Solomon, EI (2001). *J. Am. Chem. Soc.* **123**: 4938-4950.
25. Kuiper HA, Coletta M, Zolla L, Chiancone E, Brunori M. (1980) *Biochim. Biophys. Acta* **626**: 412-416.
26. Kuiper HA, Gastra W, Beintema JJ, van Bruggen EFJ, Schepman AMH et al. (1975) *J. Mol. Biol.* **99**: 619-629.
27. Kau LS, Spira-Solomon DJ, Penner-Hahn JE; Hodgson KO, Solomon EI (1987) *J. Am. Chem. Soc.* **109**: 6433-6442.
28. Blumberg WE, Eisenberg P, Peisach J, Shulman RG (1976) *Iron and Copper Proteins,* eds Yasunobu KT, Mower HF, Hayaishi O (Plenum, New York), pp 389-399.
29. Andrew CA, McKillop KP, Sykes AG (1993). *Biochim. Biophys. Acta* **1162**: 105-114.
30. Brouwer M, Bonaventura C, Bonaventura J (1978). *Biochemistry* **17**: 2148-2154.
31. Sabatucci A., Ascone I, Bubacco L, Beltramini M, Di Muro P., Salvato B (2002) *JBIC* **7**: 120-128.
32. Matoba, Y., Kumagai, T., Yamamoto, A., Yoshitsu, H., Sugiyama, M. (2006) *J. Biol. Chem.* **281**: 8981-8190.
33. Cuff ME, Miller KI, van Holde KE, Hendrickson WA (1998) *J. Mol. Biol*. **278**: 855-870.
34. Klabunde T, Eicken C, Sacchettini JC, Krebs B(1998) *Nat. Struct. Biol.* **5**: 1084-1090.
35.Beltramini, M., Colangelo, N., Giomi, F., Bubacco, L., Di Muro, P.et al. (2005) *FEBS Journal*, **272**, 2060-2075.
36. Brunori M, Zolla L, Kuiper HA, Finazzi Agrò A (1981) *J. Mol. Biol.* **153**: 1111-1123.
37. Sterner R, Decker H, (1994) *Proc. Natl. Acad. Sci. USA* **91**: 4835-4839.
38. Martin AG, Depoix F, Stohr M, Meissner U, Hagner-Holler S, Hammouti K, Burmester T, Heyd J, Wriggers W, Markl J. (2007) J Mol Biol, 366:1332-50.
39. Menze M.A., Hellmann N., Decker H., Grieshaber M.K., (2000) *Biochemistry* **39**, 10806-10811.

40. Guex, N. and Peitsch, M.C. (1997) Electrophoresis 18, 2714-2723. (http://www.expasy.org/spdbv/)

Footnotes:

‡‡ The k_{obs} value also increased on the low pH side of the minimum at 6.5 (Fig. 3A) as has been noted before for an analogous arthropod Hc (23). This phenomenon is not analyzed further.

Acknowledgements

This work was partially supported by Grants-in-Aid for Scientific Research from MEXT (Priority Areas, Nos. 18031038 and 20051016, S.H.), JSPS (Category C, No. 19550169, and the 21st COE Program (S.H.)), JST (S.H.), and by the "Progetto di Ateneo, UniPd" FIRB and MUR(PRIN) (L.B. and M.B.), NIAID/NIH 060014 (RSM), and GM040168 (JP).

Abbreviation: Hcs; Hemocyanins; XANES, X-ray Absorption Near Edge Spectroscopy; XAS, X-ray Absorption Spectroscopy; CT, charge transfer, SOD, superoxide dismutase

Figure Legends

Figure 1: oxyHc active site structure drawn from the x-ray crystal structure coordinates of *L. polyphemus* Hc (1OXY.pdb); The software PDBviewer (40) was used to illustrate the structures.

Figure 2: Flash-photolysis measurements of *C. aestuarii* oxyHc. Absorbance changes at 337 nm by 355-nm pulse irradiation under various oxygen concentrations are shown. Single exponential best-fitted curves are indicated by red lines. Experimental conditions: 20 μM Hc; 20 mM Ca^{2+}, 50 mM Tris-HCl buffer, pH 8.3; laser pulse, 30 mJ, 10 Hz; 20°C; [O_2], 0.07, 0.14, 0.21, 0.28, 0.35, 0.49, 0.70, 0.91, 1.11, and 1.39 mM (remaining gas is N_2). Each trace is an average of 512 shots. (Inset) Wavelength dependence of the initial absorbance changes at the indicated wavelengths (circles) superimposed on the difference absorbance spectrum (red line, oxyHc minus deoxyHc).

Figure 3: (A) Oxygen binding rate constants for *C. aestuarii* Hc at pH 5.6 to 8.7. Acetate, MES, and Tris-HCl buffers (50 mM), were used for measurements at pH 5.6, 6.0–6.5, and 7.1–8.7, respectively. (B) Plots of k_{obs} vs [O_2] for the reaction of Hc with oxygen at pH 8.3 (black) and 6.5 (red), together with the least-squares-fitted line according to eq. 1. Experimental conditions are the same as those listed in Fig. 2.

Figure 4: Temperature dependence (5–25°C) of oxygen binding rate constants for *C. aestuarii* Hc. Experimental conditions are the same as those in Fig. 2, except Tris-HCl buffer, pH 7.8, was used. k_B is the Boltzmann constant.

Figure 5: k-Edge x-ray absorption spectra of *P. interruptus* Hc. a) DeoxyHc, b) oxyHc, and c) difference spectrum obtained by subtraction of the oxyHc spectrum from the deoxyHc spectrum. Both experimental spectra were collected from samples in 50 mM Tris-SO_4 buffer, pH 9, containing 20 mM $CaCl_2$.

Figure 6**:** k-Edge x-ray absorption spectra of *P. interruptus* deoxyHc. a) pH 5 in 50 mM acetate buffer, b) pH 7 in 50 mM Tris-SO_4 buffer, c) pH 9 in 50 mM Tris-SO_4 buffer. $CaCl_2$ (20 mM) was present in all samples.

Figure 7**:** k-Edge x-ray absorption spectra of subunit II of *L. polyphemus* deoxyHc. a) pH 6 in 10 mM Tris-SO_4 buffer, b) pH 9 in 100 mM Tris-SO_4 buffer, c) pH 9 in 50 mM Tris-SO_4 buffer plus 500 mM NaCl, d) pH 6 in 50 mM Tris-SO_4 buffer plus 500 mM NaCl. $CaCl_2$ (20 mM) was present in all samples. The buffer concentration for a and b were chosen to compensate for ionic strength effects.

Figure 8: Reaction scheme for oxygenation of arthropod hemocyanin including a change in geometry of copper in the deoxygenated active site with pH. A) (Square pyramidal) oxyHc active site structure drawn from the x-ray crystal structure coordinates of *L. polyphemus* Hc (1OXY.pdb); B) (Trigonal) active site of *P. interruptus* deoxyHc (1HCY.pdb) assumed here to be representative of the low pH form. C) (Pseudotetrahedral) active site of *L. polyphemus* deoxyHc (1LLA.pdb) assumed to closely represent the alkaline pH form. The software PDBviewer (40) was used to illustrate the structures. The k_{on} and k'_{on} represent the on-rates discussed in the text for the high and low pH conditions.

Table I: Values of p_{50} for oxygen binding to Hcs as a function of pH in the presence of 10 mM $CaCl_2$.

	PH	P_{50} O_2 mmHg
P. interruptus	5.25 7 9	172[a] 42[b] 5[b]
C. aestuarii	7.1 7.5 7.9 8.3	44.3[c] 33.7[c] 13.6[c] 6.81[c]
Subunit II *L. Polyphemus*	7 9	2.5[d] 1.4[d]

a) In 100 mM Bis-Tris, pH 5.25 (30); b) In 50 mM Tris-HCl, pH 7 and in 50 mM ethanolamine, pH 9 (31); c) In 50 mM Tris-HCl (1); d) In 100 mM Tris-HCl, pH 7 and 9 (23).

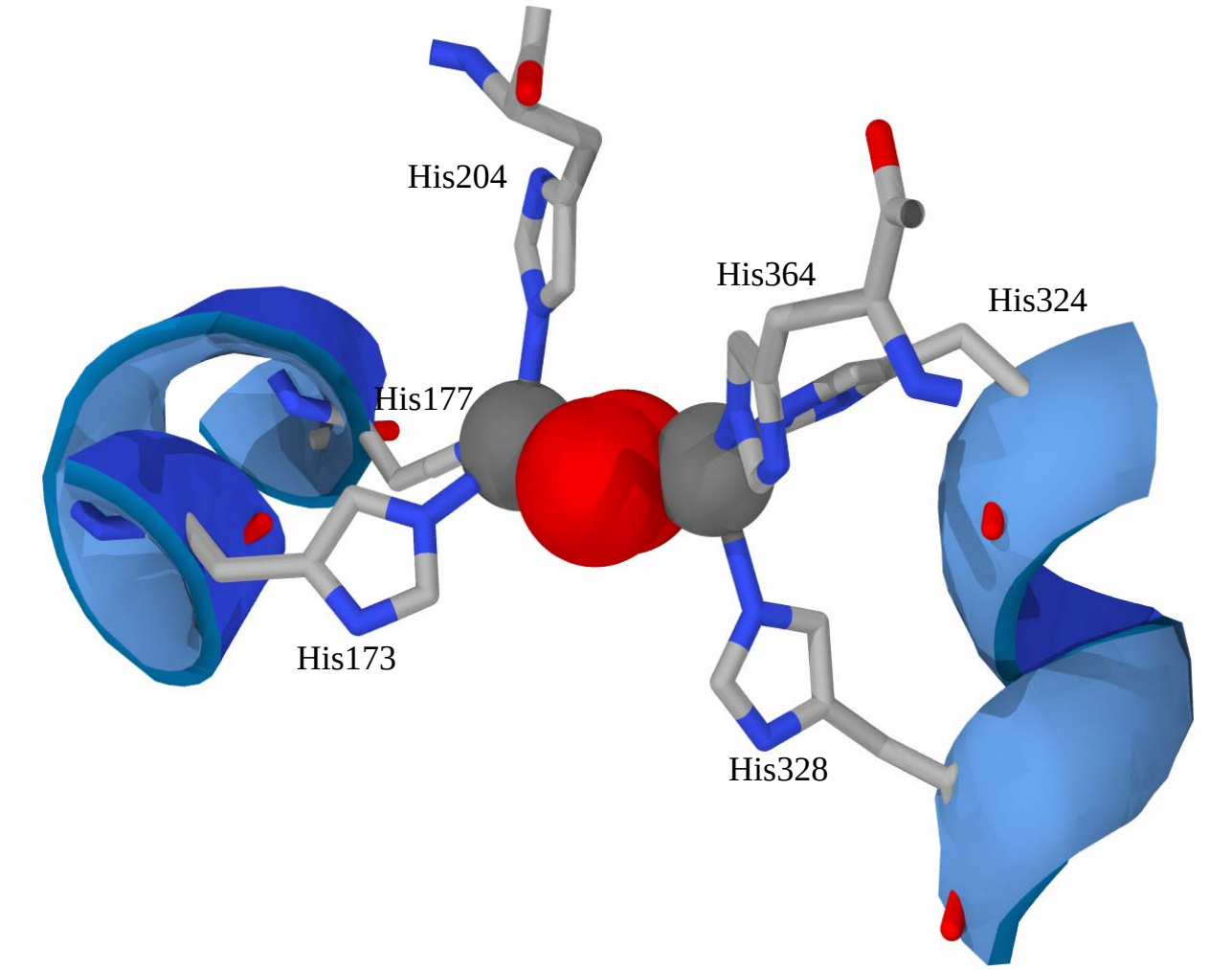

Hirota et al., Figure 1

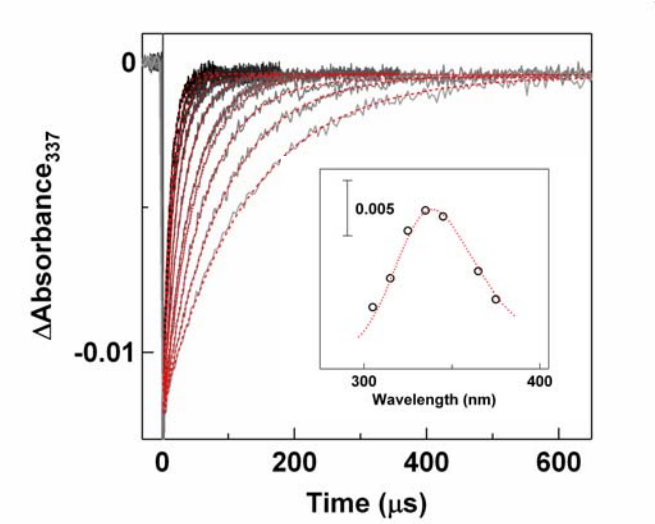

Figure 2 (Hirota et al.)

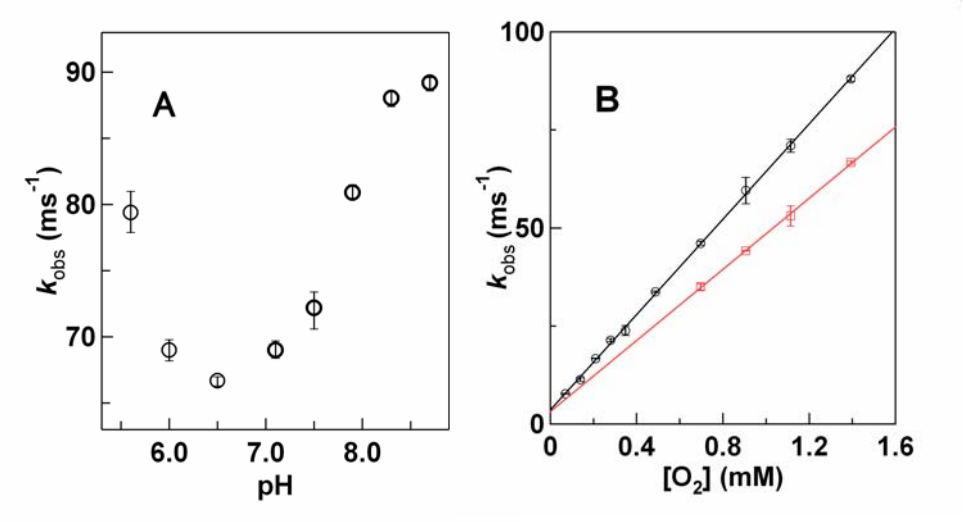

Figure 3 (Hirota et al.)

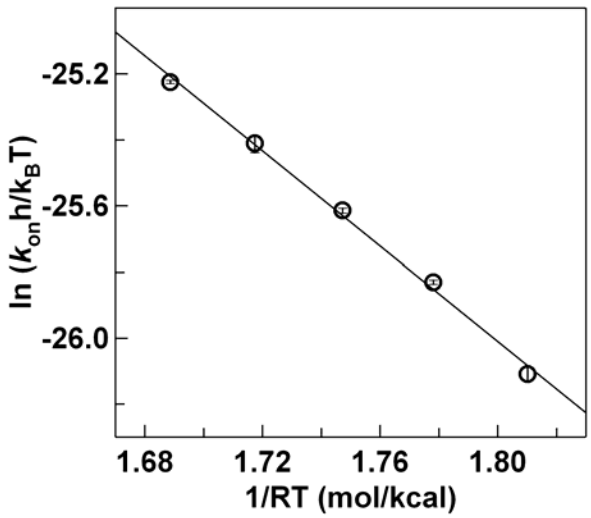

Figure 4 (Hirota et al.)

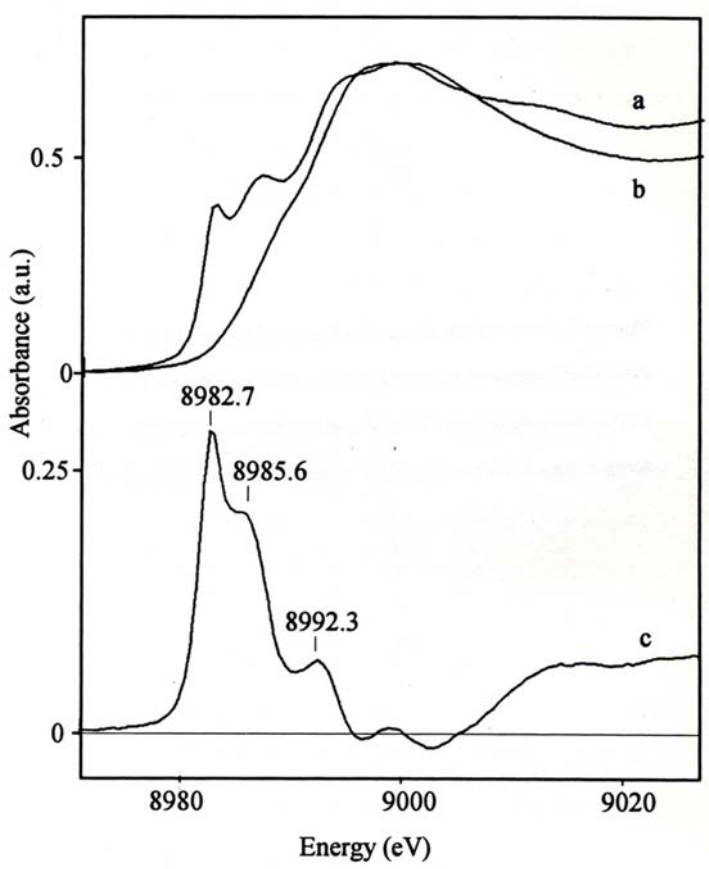

Figure 5 (Hirota et al.)

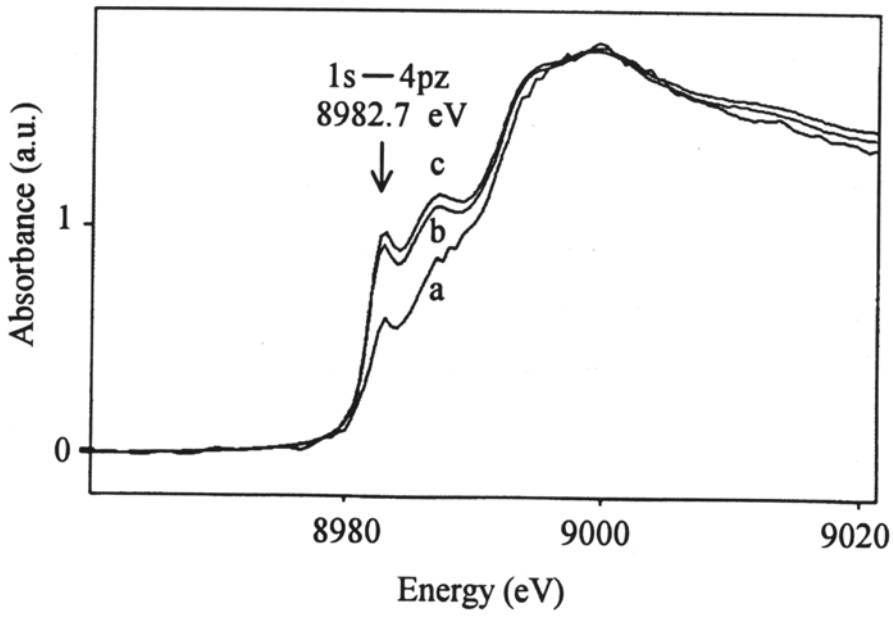

Figure 6 (Hirota et al.)

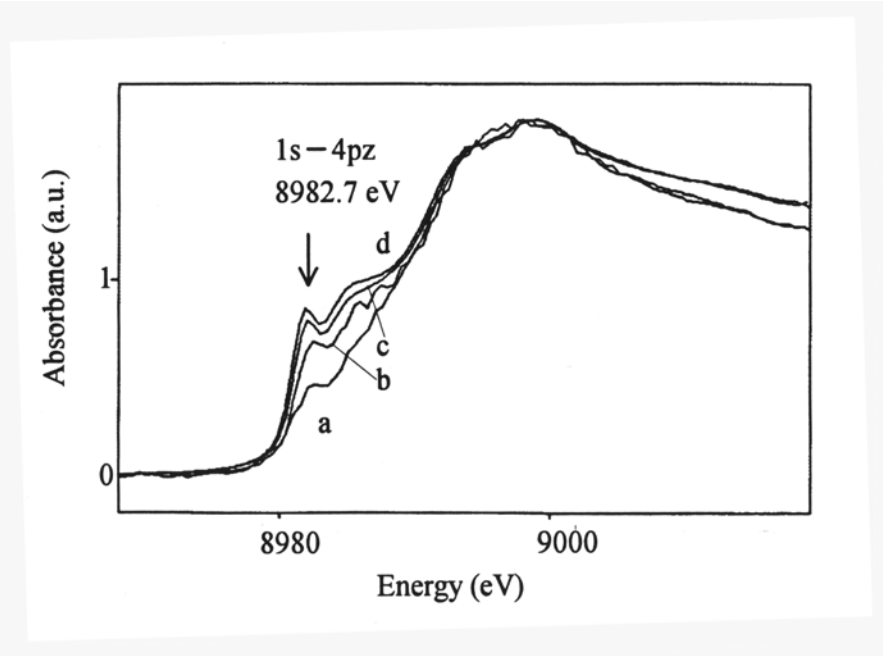

Figure 7 (Hirota et al.)

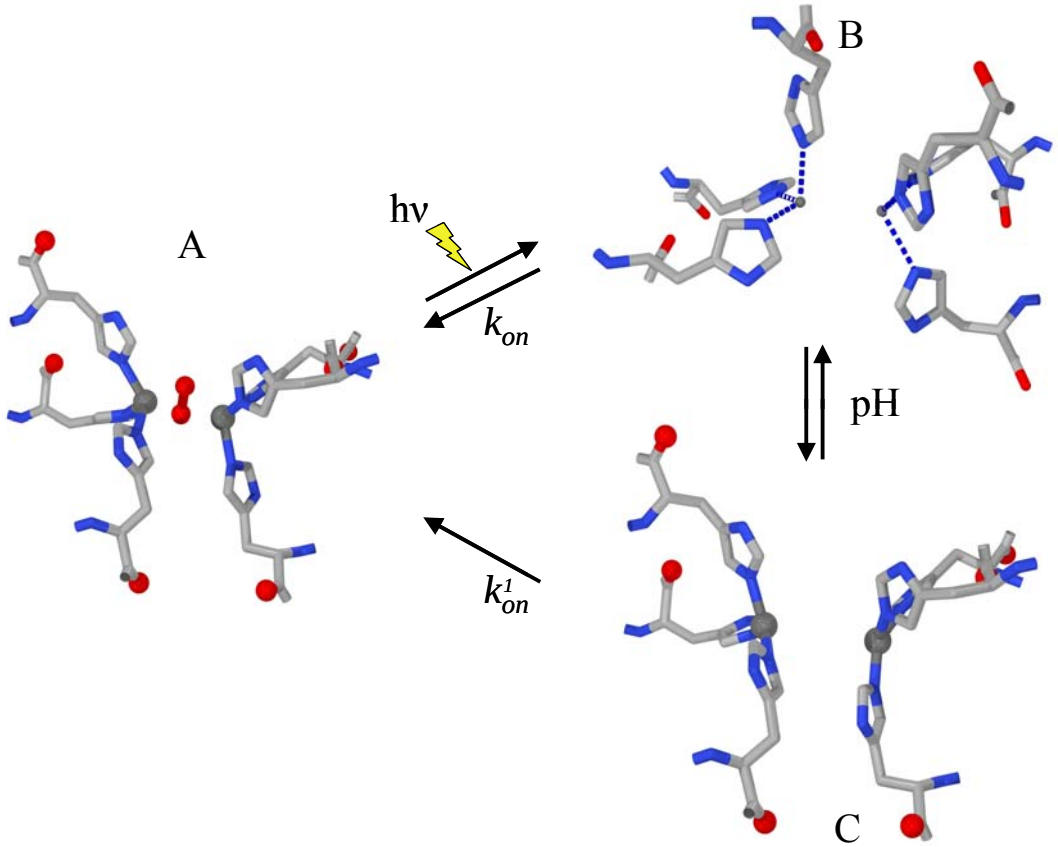

Figure 8 (Hirota et al.)

Supporting Information

MOLECULAR BASIS OF THE BOHR EFFECT IN ARTHROPOD HEMOCYANIN

Shun Hirota[1,2], Takumi Kawahara[2], Mariano Beltramini[3], Paolo Di Muro[3], Richard S. Magliozzo[4], Jack Peisach[5], Linda S. Powers[6], Naoki Tanaka[1], Satoshi Nagao[1], and Luigi Bubacco[3]

[1] Graduate School of Materials Science, Nara Institute of Science and Technology, Nara, Japan; [2] Department of Physical Chemistry and 21st Century COE Program, Kyoto Pharmaceutical University, Kyoto, Japan; [3] Department of Biology, University of Padova, Padova, Italy; [4] Department of Chemistry, Brooklyn College, Brooklyn, NY, USA; [5] Department of Physiology and Biophysics, Albert Einstein College of Medicine, Bronx, NY, USA; [6] National Center for the Design of Molecular Function, University of Arizona, Tucson, AZ USA.

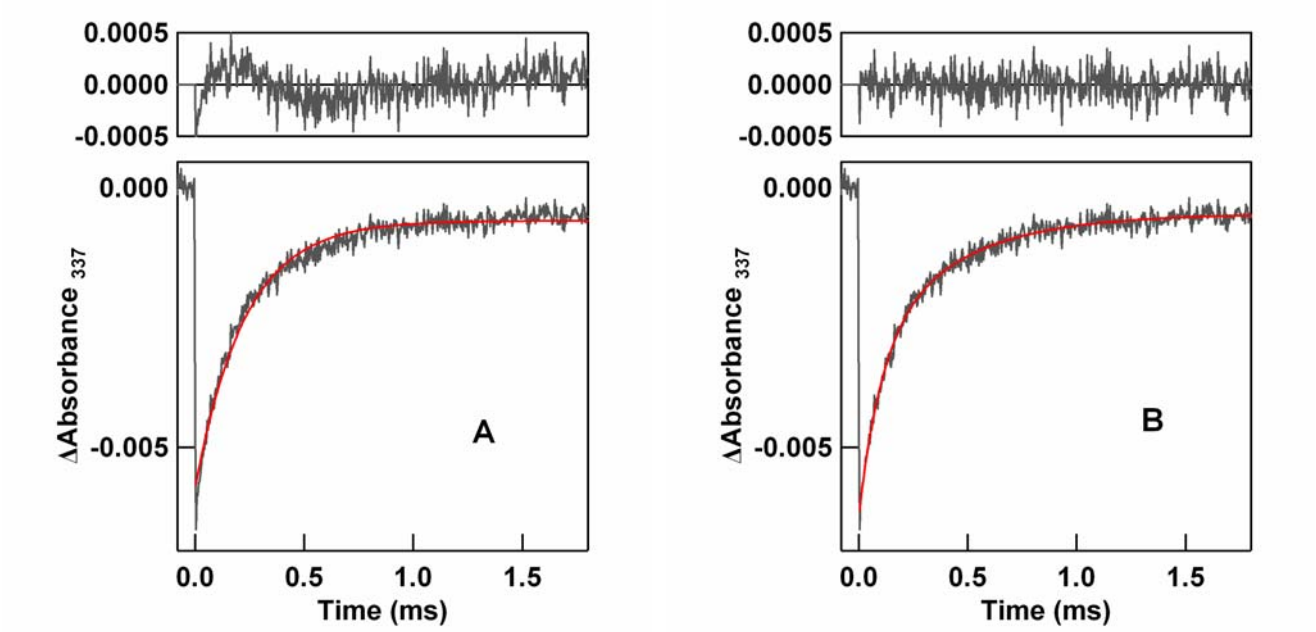

Figure S1. Time-resolved absorbance change of *C. aestuarii* oxyHc obtained by 355-nm pulse irradiation at pH 7.1 under 10% oxygen with 90% nitrogen, together with the least-squares-fitted single (A) and double (B) exponential curves (red lines) and their residuals. The trace is an average of 256 shots. Note that the fitting is not successful for the single exponential.

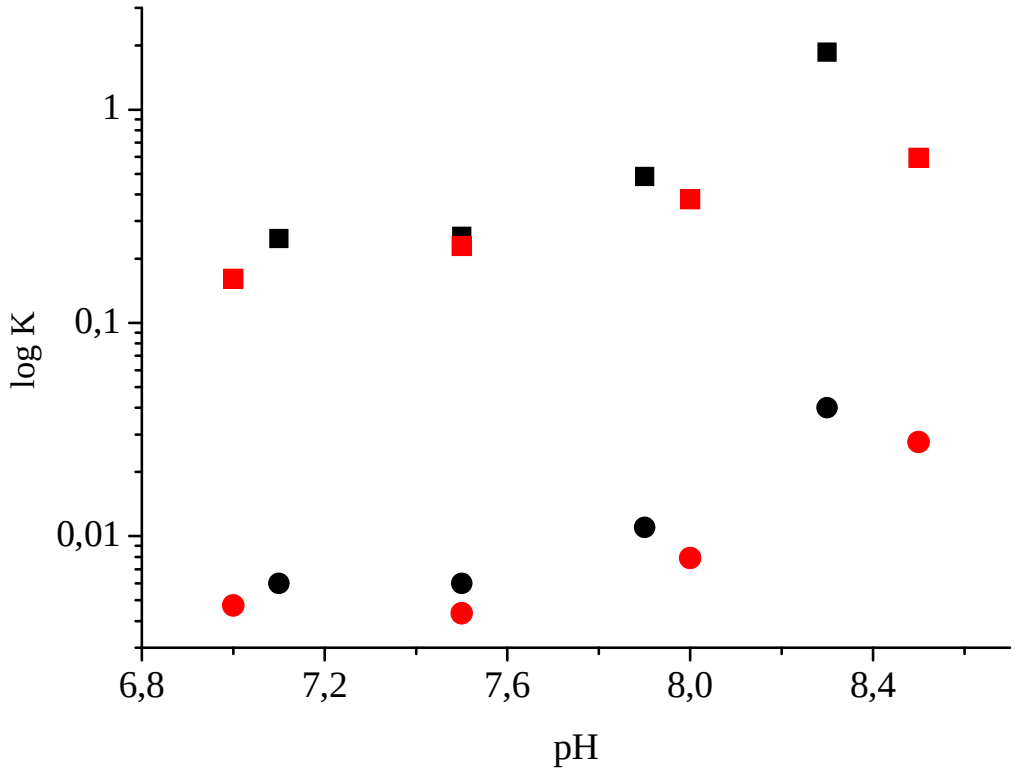

Figure S2 pH dependence of K_R (squares) and K_T (circles) for *Carcinus aestuarii* Hemocyanin (Black) and *Penaeus monodon* Hemocyanin (Red). The data for *Carcinus aestuarii* Hemocyanin are plotted after Table 1 of reference 1 and the data for *Penaeus monodon* Hemocyanin are plotted after Table 3 of reference 35 in the manuscript. These data for both *Carcinus aestuarii* and *Penaeus monodon* Hcs show that the pH dependence of K_T and K_R has a very similar profile.